Structure and Tensile Properties of Nanoclay–Polypropylene Fibers Produced by Melt Spinning

Loganathan Rangasamy, Eunkyoung Shim, Behnam Pourdeyhimi

College of Textiles, North Carolina State University, Raleigh, North Carolina 27695-8301

Received 16 March 2010; accepted 17 October 2010
DOI 10.1002/app.33619
Published online 18 February 2011 in Wiley Online Library (wileyonlinelibrary.com).

ABSTRACT: Nanocomposite fibers of polypropylene and montmorillonite-based organoclay were produced by a melt-spinning process, and their structures and mechanical properties were studied. The addition of nanoclay in polypropylene increased the rate of crystallization and altered the microstructures of the fibers. Increases in the crystal size and a reduction in the molecular orientation were observed in the nanoclay–polypropylene composite fibers. The tensile properties of nanoclay composite fibers were also studied, and decreases in the fiber modulus and tenacity and increases in the strain at break were observed. © 2011 Wiley Periodicals, Inc. J Appl Polym Sci 121: 410–419, 2011

Key words: additives; extrusion; fibers; nanocomposites; poly(propylene) (PP)

INTRODUCTION

One of the interesting developments of nanomaterials in polymer engineering is that of nanoclay particulate additives. Nanoclay-based additives have shown great potential in polymer and plastic applications because they overcome many limitations of traditional microcomposites. Many previous studies have demonstrated their excellent properties, including superior balance of modulus, impact strength, improved thermomechanical performance, fire resistance, and enhanced barrier properties.[1–5] The reason behind these unique behaviors is the nanostructures created by the nanoclay layer/polymer molecular chain.

The structures of nanoclay–polymer composites can be classified by their degree of dispersion.[6,7] Traditional microcomposites [Fig. 1(a)] are formed when the polymer chain is unable to penetrate between the silicate layers. As the results, the clays forms relatively large aggregates as a separate phase inside the host polymer matrix, which forms continuous phase. Improved rigidity can be achieved with this type of composite, but there are reductions in the elongation and toughness. An intercalated structure is formed when a single or more extended chain is intercalated between the nanoclay silicate layers; this results in a well-ordered multilayer with alternating polymeric and inorganic clay layers [Fig. 1(b)]. The structure with the highest degree of dispersion is called an *exfoliated* or *delaminated structure,* where the silicate layers are completely opened up and dispersed in a disorderly and uniform manner in a continuous polymer matrix [Fig. 1(c)]. Both intercalated and exfoliated structures are considered nanocomposites, which can provide significant performance enhancements.[7]

Nanoclay particles have high surface-area-to-volume ratios and their sizes are similar to the segment of the surrounding polymer chains in nanocomposites; this makes it possible for the nanoclay particles to form significant bonding with the polymer matrix.[3] This may lead to improvements in many of the polymer properties, and nanoclays have been reported to be excellent reinforcement additives. Increases in the tensile strength, modulus, and crack resistance have been achieved, even at low concentrations.[2] A reduction in the creep behavior has also been found in some nanoclay–polymer composites.[4] A higher nanoclay loading does not always improve the mechanical properties, but property degradation due to the coagulation of nanoclays has been observed.[2] The ability to achieve good performance at a low inorganic loading can provide an added advantage: a lighter reinforced composite. Nanoclays also impart outstanding diffusional barrier properties, enhanced chemical resistance, and flame retardancy.[1,5]

Nanoclay–polymer composite structures are highly dependent on the preparation process and conditions, polymer–nanoclay interaction, and the presence of other chemicals, such as compatibilizers.[8,9] The achievement of proper polymer–nanoclay interactions has been an important issue in nanocomposite

Correspondence to: E. Shim (eshim@ncsu.edu).
Contract grant sponsor: Nonwovens Cooperative Research Center (North Carolina State University, Raleigh, NC).

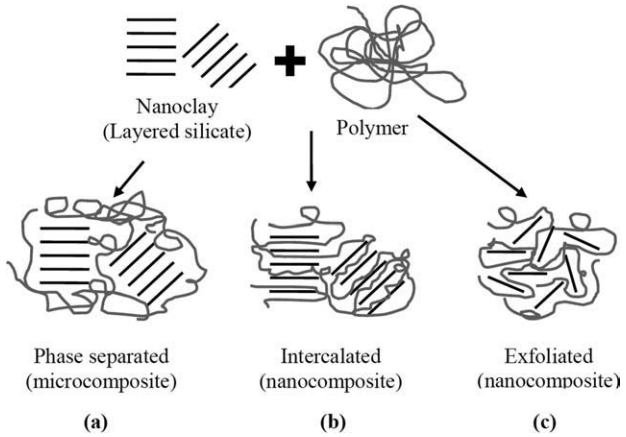

Figure 1 Classification of the nanoclay–polymer composite structures.[6,7]

development. The silicate surface of the nanoclay is hydrophilic in nature, and it hinders homogeneous dispersion in organic polymer matrixes. To achieve the required properties, a good dispersion of nanoclay in the polymer matrix and a good interface between the two phases are essential.[10] One way to improve the compatibility between the hydrophilic inorganic clay and the oleophilic organic polymer is to modify the surface of the clay through an ion-exchange reaction. This involves the exchange of hydrophilic cations on the clay surface with short-chain organic cations, such as alkyl ammonium ions.[11,12] The surface modification of clay, often referred to as *organoclay*, has shown improved compatibility with the polymeric matrix.[8,11]

In some polymer matrixes, especially highly hydrophobic polyolefin polymers, organoclay could still not provide enough nanoclay–polymer interactions to produce a high degree of clay dispersion. The use of compatibilizers, such as maleic anhydride modified polypropylene (PP), have been reported, and the use of this method has caused improvements in the clay dispersion and the mechanical properties.[2,13–16]

There are three types of preparation methods for polymer/nanoclay composites: *in situ* polymerization, the solution method, and melt blending. One of the earliest methods used in the Toyota laboratory was *in situ* polymerization, where the polymerization reaction of a monomer occurred in the presence of nanoclay. The solution process may provide a better and more stable dispersion of nanoclay in host–polymer matrix, but more complex process steps are involved, and it also considered environmentally unfriendly.[17] Melt blending is believed to be most convenient preparation process, and traditional polymer process equipment can easily be used. However, some researchers have reported that nanoclays prepared with melt blending can be unstable for reprocessing and high-processing temperatures may transform the nanocomposite into microcomposites.[17]

Despite recent increasing interest in nanoclay, most studies have concentrated on films and plastic molds, and we found only a few studies on nanoclay-modified fibers.[18] Compared to films, fiber-based systems are known to provide many beneficial characteristics because of their high surface areas, so a combination of nanocomposite technology and fiber formation is highly sought after. However, melt spinning is a more complex process, where fiber fine structure development is determined by polymer-chain responses to tension, temperature, and shear deformation in the spin line. It has been reported that nanoclay incorporation alters the polymer melt rheology and crystallization kinetics,[19–22] which are the key factors affecting microstructure formation during the fiber melt spinning. Several authors have reported nanoclay–polymer composite fiber properties, but their findings have been contradictory and fragmented at best.[16,18,23] Because the properties of polymeric fibers are highly influenced by the microstructures of how the polymer chains are aligned, to further determine the effect of nanoclay addition on melt-spun systems, one should look not only at the dispersion of nanoclay layers in polymeric materials but also at their impact on the fiber-forming mechanism and the crystalline structures of fibers related to their properties.

In this study, nanocomposite fibers of PP and montmorillonite-based organoclay were produced by a melt-spinning process, and their structures and mechanical properties were investigated.

EXPERIMENTAL

Materials

Spunbond-grade PP (PP CP360H), with an average melt flow rate of 35 g/10 min, was supplied by Sunoco Chemicals (Philadelphia, PA). A commercially available, precompounded, montmorillonite-based organoclay–PP (Nanomax PP) was purchased from Nanocor (Arlington Heights, IL).

Nanomax PP contained about 50% Nanomer nanoclay (i.e., surface-modified montmorillonite clays), PP, and a maleic anhydride modified polyolefin compatibilizer and was prepared by melt compounding, on the basis of patented technology,[24,25] to produce intercalated structures.

Melt spinning of the nanoclay–PP composite fibers

Even Nanomax PP precompounded masterbatch pellets containing PP, nanoclay, and compatibilizer and good processability were reported in various plastic processing equipment, our initial attempt to

spin the composite fibers by the direct mixing of Nanomax PP and PP and extrusion in fiber-spinning equipment caused a series of spinning problems, including melt fractures, filter blockages, spin-line breakages, and large agglomeration of the clay particles. Therefore, Nanomax PP and PP were melt-compounded further to reduce the clay loading. Nanoclay–PP composite pellets with nanoclay loadings of 5 wt % were prepared by melt compounding at 205°C in a TechmerPM (Clinton, TN). Then, nanoclay–PP composite pellets were again mixed and extruded with PP to produce nanoclay–PP composite fibers with the Hills Homofilament Research line in the Nonwovens Institute, North Carolina State University (Raleigh, NC). The spinning speed was 2000 m/m, and the spin-head temperature was 265°C. A melt throughput was maintained at 1 g hole^{-1} min^{-1}. Nanoclay–PP fibers with a clay load of 0.5–3% were produced. As a control, PP without nanoclay was melt-extruded under the same conditions. The fiber sizes of all of the samples were about 5 denier.

Transmission electron microscopy (TEM)

Cross sections of the nanoclay–PP composite fibers were investigated under a Hitachi HF 2000 transmission electron microscope to study the nanoclay dispersion in PP. We prepared the samples by embedding the fiber samples in Spurr's epoxy and microtoming them to 70 nm thick.

Differential scanning calorimetry (DSC)

The melting and crystallization behaviors of the composite were analyzed with a PerkinElmer differential scanning calorimeter (Perkin Elmer, Norwalk, CT). Nanoclay–PP composite fibers (4.5 ± 0.5 mg) were heated in a nitrogen atmosphere from 25 to 190°C and allowed to stand for 10 min at 190°C and then cooled from 190 to 25°C. In all cases, the heating/cooling rate was maintained at 5°C/min.

The crystallinity of the samples was calculated with the following formula:

$$\text{Crystallinity } (\%) = \frac{\Delta H}{\Delta H^0_{\text{PP}}} \times 100 \tag{1}$$

where ΔH is the enthalpy of fusion of the sample (J/g) and ΔH^0_{PP} is the enthalpy of fusion of the completely crystalline PP (~ 207 J/g).[26]

Isothermal crystallization

The isothermal crystallization of the nanoclay–PP composites were also investigated with the PerkinElmer differential scanning calorimeter. The samples were heated at a rate of 20°C/min to 190°C and kept at 190°C for 10 min; then, they were cooled down at a rate of 50°C/min to crystallization temperatures ranging from 124 to 128°C and allowed to crystallize there for 10 min.

Birefringence

The birefringence of the fibers was measured with an Aus Jena Interference microscope. The wavelength of the polarized light used was 546 nm. The fibers were immersed in oil with a matching refractive index (Cargill), and the refractive indexes parallel and perpendicular to the fiber axis were measured from the interference fringe shifts.

Then, the birefringence of the samples was calculated with the following formula:

$$\text{Birefringence} = |n_{\parallel} - n_{\perp}| \tag{2}$$

where $n_{\parallel}$ is the refractive index of the sample parallel to the direction of orientation and $n_{\perp}$ is the refractive index of the sample perpendicular to the direction of orientation.

Wide-angle X-ray diffraction (WAXD)

The crystallinity and crystal size of the samples was calculated with an Omni Instrumental X-ray diffractometer (Biloxi, MS). The diffractometer was equipped with Be-filtered Cu Kα radiation with a wavelength of 1.54 Å and generated at 35 kV and 25 mA. The fiber samples were wound onto the sample holder and placed in the sample holder. The samples were scanned in the 2θ range 3–30° with an increment of 0.05°. From the scattering pattern, the crystal sizes of the samples were calculated with Scherer's equation:[27]

$$t = \frac{0.9 \times \lambda}{B \times \cos\theta_B} \tag{3}$$

where t is the crystal size (Å), λ is the X-ray wavelength (1.54 Å), B is the full width at half-maximum (rad), and θ_B is the Bragg angle (°).

Single-fiber tensile properties

The single-fiber tensile properties of the nanoclay–PP composite fibers were evaluated according to ASTM D 3822-07 in an Instron MTS instrument with a 50-g load cell (Canton, MA). The gauge length was 2.54 cm, and the rate of extension was 15 mm/min. The tenacity, secant modulus at 5% strain, toughness, and strain at break were calculated from the tensile stress–strain curve, and the average of 10 samples are reported.

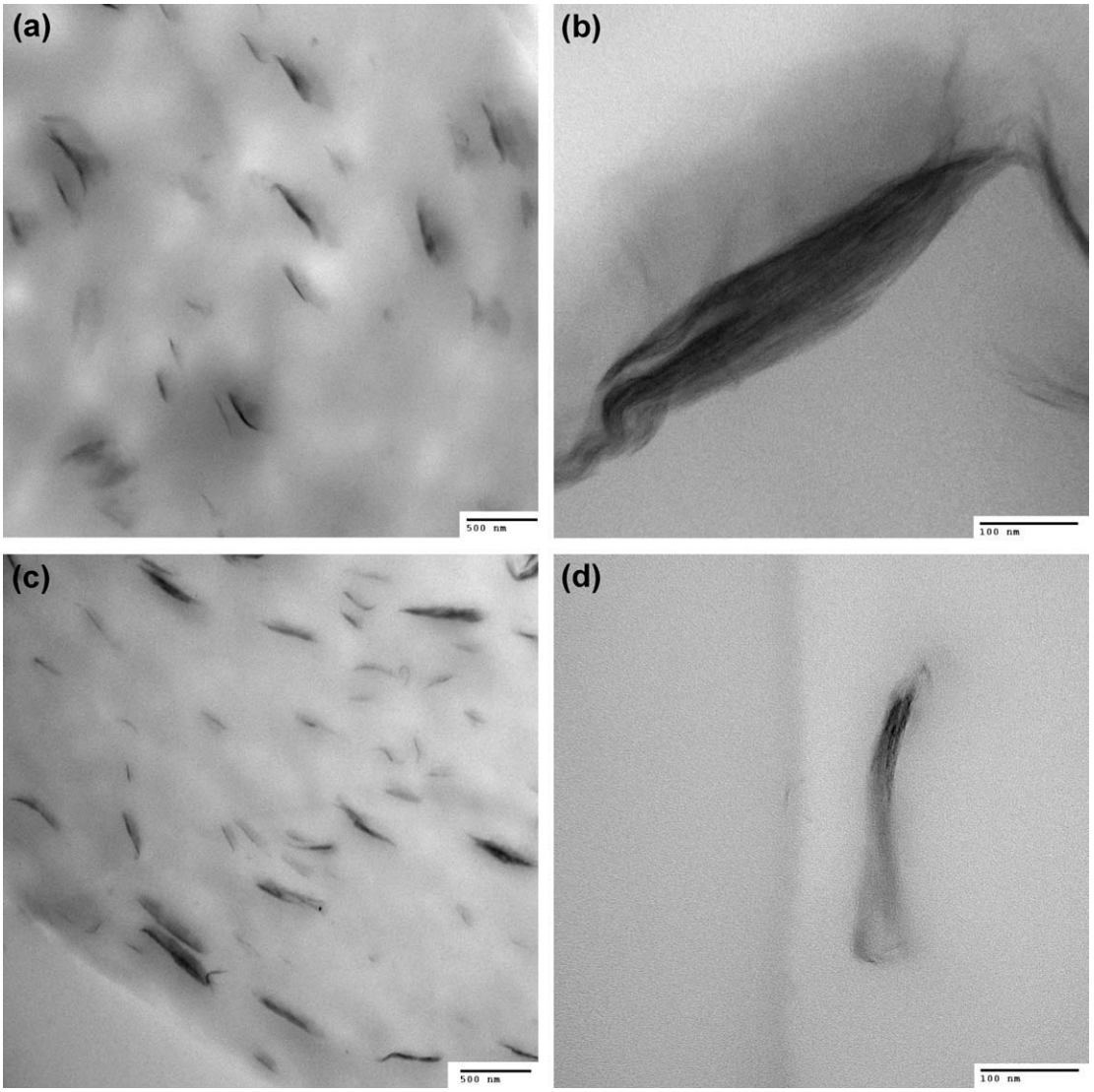

Figure 2 TEM images of cross sections of nanoclay–PP composites fibers with nanoclay concentrations of (a) 1% (8000× magnification), (b) 1% (60,000× magnification), (c) 3% (8000× magnification), and (d) 3% (60,000× magnification).

RESULTS AND DISCUSSION

Nanoclay dispersion in the PP fibers

TEM images of the nanoclay–PP fiber cross sections showed that the nanoclay layers were uniformly distributed at both 1 and 3% clay loadings [Fig. 2(a,c)]. It was apparent that the nanoclay platelets were stacked to thickness ranges of 10–100 nm, and the thickness of the platelet stacks was not affected by the nanoclay loading. Observations at higher magnifications revealed more details of the nanoclay platelet arrangements in the polymer matrix. It was very apparent that dark clay platelets and thin polymer layers were alternating, and this confirmed that the nanoclay platelets and host polymers were well intercalated. However, there were dark areas where clay layers were aggregated without polymer chain penetrating between the layers. In addition, areas where platelets were arranged in a less ordered manner were also observed; this suggested the possible presence of exfoliated structures in the fibers. No significant effect of clay loading on the clay platelet distribution was observed.[28]

DSC analysis

As illustrated in Figure 3, nanoclay addition affected the thermal transition temperature, both in the heating and cooling processes. The melting endotherm, shown in Figure 3(a), indicated a slight increase in the melting temperature. It was even more interesting that changes in the shape of the melting endotherm implicated a possible alteration of the fiber microstructure as the result of nanoclay addition, although there were few changes in the overall crystallinity. The melting endotherm of the PP control

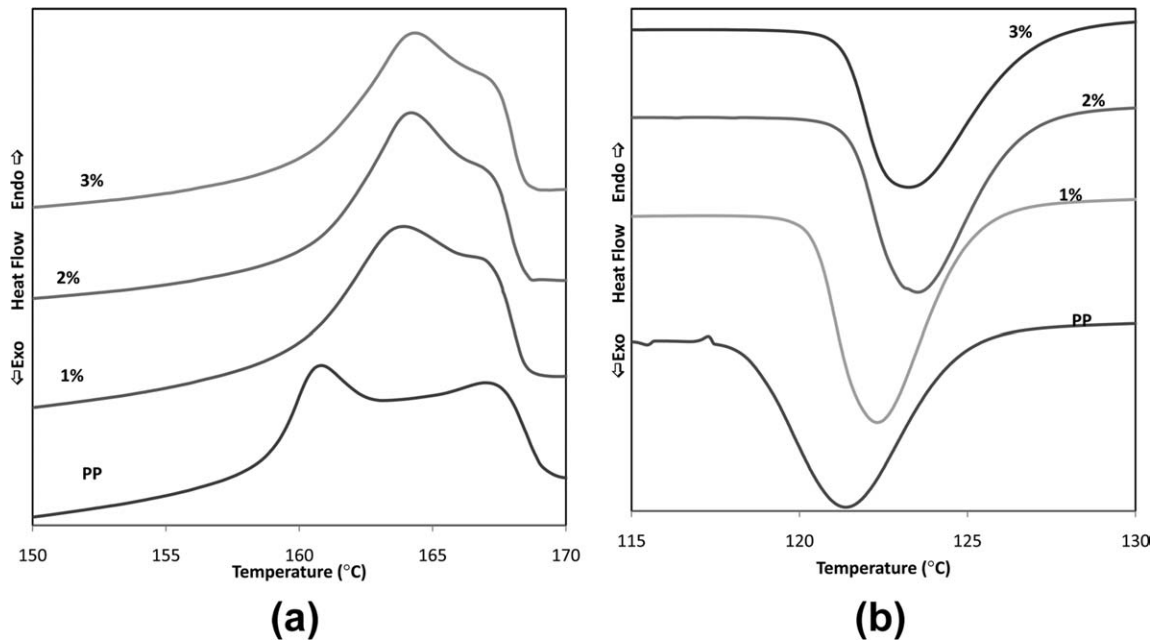

Figure 3 DSC thermograms of nanoclay–PP composite fibers: (a) heating thermogram of the melting endotherm and (b) cooling thermogram of the crystallization exotherm.

fibers were broad and consisted of two distinct melting peaks. The first peak, at a low melting point, indicated the presence of small and imperfect crystallites. When nanoclay particles were present, the melting peaks became narrower, and the two peaks became less distinct. This indicated that they had narrower ranges of crystal sizes. A slight increase in the melting temperature with increasing clay loading suggested that the crystallites became larger and more perfect (Table I). However, there were few changes in the overall crystallinity measured from the total area of the melting endotherm (Table I).

This may have been due to an alteration in the crystallization behavior, as observed in Figure 3(b). The onset crystallization temperatures detected in the DSC cooling curve increased slightly in the Nanomax PP samples. The area of the crystallization peak in the cooling curve further converted to relative crystallinity, and the results are shown in Figure 4. It was very clear that the addition of nanoclay increased the crystallization rate. To gain more understanding of the effect of the nanoclay in the crystallization kinetics, the isothermal crystallization of the nanoclay–PP composite fibers was studied, and the results are reported in the next section.

Isothermal crystallization

The isothermal crystallization kinetics of the nanoclay–PP composite fibers at different crystallization temperatures were analyzed according to the Avrami equation.[29,30]

$$1 - X_t = \exp(-kt^n) \text{ or}$$
$$\ln[-\ln(1 - X_t)] = n \ln t + \ln k \quad (4)$$

TABLE I
Melting and Crystallization Temperatures and Crystallinity (%) of Nanoclay–PP Composite Fibers

Nanoclay loading	Onset crystallization temperature (°C)	Peak crystallization temperature (°C)	Onset melting temperature (°C)	First peak melting temperature (°C)	Crystallinity (%)
PP	123.8	120.2	158.4	161.0	50
0.5%	124.7	121.5	159.3	163.1	49
1.0%	124.8	121.6	159.4	163.9	49
1.5%	125.3	121.8	160.3	163.8	47
2.0%	126.5	123.5	160.3	164.2	49
2.5%	126.7	123.2	160.3	164.4	47
3.0%	126.8	123.3	160.2	164.3	47

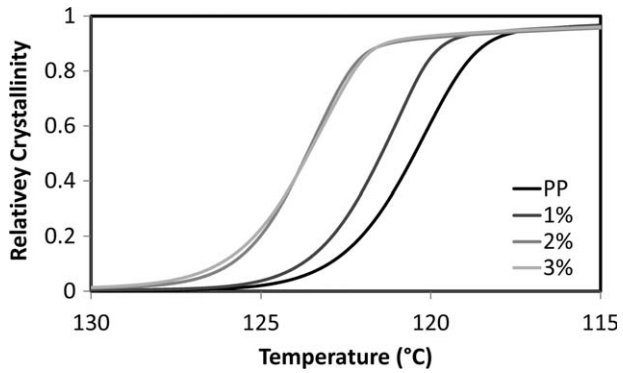

Figure 4 Nonisothermal crystallization of nanoclay–PP at a cooling rate of 5°C.

where X_t is the relative crystallinity at crystallization time t, k is the crystallization rate constant, and n is the Avrami exponent.

Avrami plots of $\ln[-\ln(1 - X_t)]$ versus $\ln t$ of 1% nanoclay–PP fibers and the PP control fibers are shown in Figure 5. From these Avrami plots, n and k values were obtained from the slope and intercept of the linear line fitting, and the results are given in Table II. In the entire crystallization temperature range studied, 1% nanoclay addition led to an increase in k and reductions in the crystallization half-time. This indicated faster crystallization in the samples with added nanoclay. This result agreed well with those of other studies.[19–22] Ma et al.[19] and Zhang et al.[20] concluded that the exfoliation of silicate layers results in an increase in the number of heterogeneous nuclei and, thus, increases the crystallization rate. Therefore, the presence of clay particles acted as a heterogeneous nucleating agent and led to a higher crystallization rate, and the crystallization of the PP–clay-added composite fiber samples followed the heterogeneous nucleation mechanism. This was further supported by n, also given in Table II. The n value is an indicator of the crystal growth mechanism. In the PP polymer, n was around 3.5–3.6; this value represented spherulite crystalline growth and some nucleating. With a 1% addition of nanoclay, the n values increased to 3.6–3.9 with increasing heterogeneous nuclei formation. Therefore, the nanoclay particles acted as a heterogeneous nucleating agent in the polymer matrix and increased the crystallization rate of the host polymer.

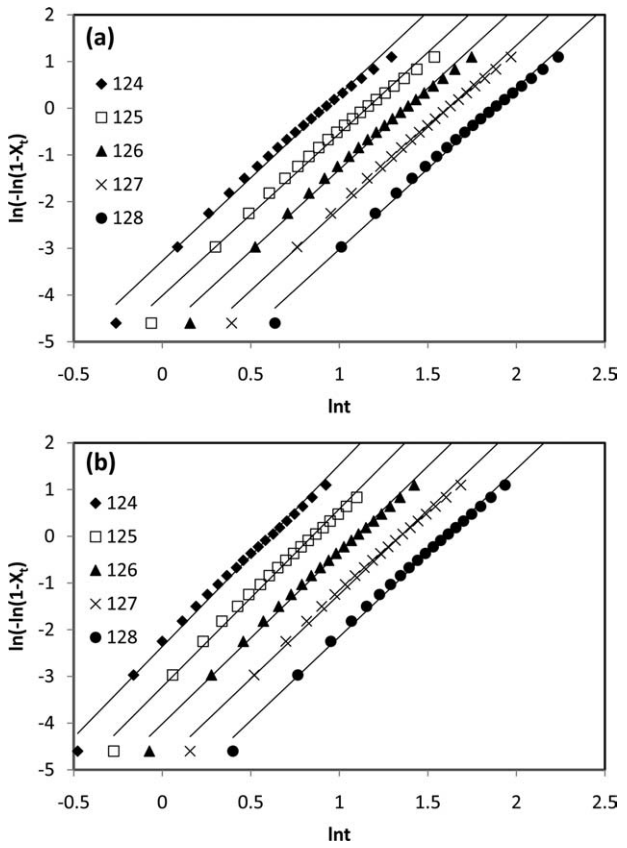

Figure 5 Avrami plots of $\ln[-\ln(1 - X_t)]$ versus $\ln t$ for (a) PP and (b) 1% nanoclay–PP.

Fiber formation during melt spinning is the process of phase transition from an entangled polymer melt to ordered semicrystalline materials with complex microstructures. Because the crystallization behavior of materials greatly affects the fiber fine structures developed during melt spinning, changes in the crystallization kinetics with the addition of nanoclay can lead to significant changes in the microstructure of fibers.

TABLE II
Kinetic Parameters of the Isothermal Crystallization of Nanoclay–PP Composite Fibers with a 1% Nanoclay Concentration

		Crystallization temperature (°C)				
Sample	Parameter	124	125	126	127	128
PP	Half-time (min)	2.22	2.80	3.51	4.47	5.78
	n	3.56	3.47	3.48	3.50	3.46
	k	0.0381	0.0181	0.0082	0.0035	0.0015
1% nanoclay	Half-time (min)	1.65	2.10	2.67	3.43	4.42
	n	3.89	3.81	3.68	3.61	3.59
	k	0.0944	0.0398	0.0180	0.0078	0.0032

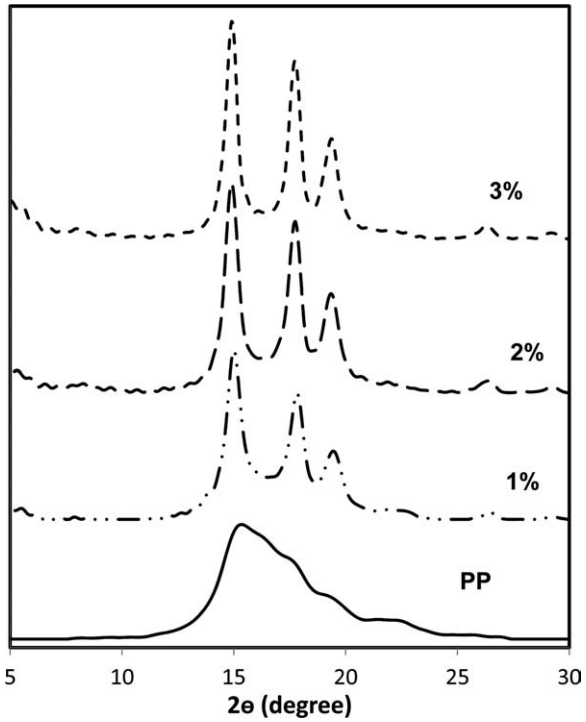

Figure 6 X-ray diffractograms of PP and nanoclay–PP composite fibers.

Crystalline structures: WAXD

Nanoclay particles added in the melt-spinning process affects the fiber-formation process and the fiber fine structures. Changes in the crystalline morphology were observed with WAXD. The X-ray diffractogram of pure PP showed a broad crystalline peak at a 2θ value of 15.1; this corresponded to the mesomorphic form of isotactic PP (Fig. 6). The crystalline peaks were not well defined, so this indicated imperfect and not well-defined crystalline structures of the PP fibers. When nanoclay was added to the fibers, the crystalline peaks were sharper and more distinct. In the case of the addition of 1% nanoclay–PP fibers, distinct crystalline peaks occurred at 2θ values of 15.0, 17.8, 19.5, 22.1, and 26.4; this corresponded to the α-crystalline form of isotactic PP. As the percentage of clay loading increased, the positions of the crystalline peaks did not changes, but the peaks became shaper. This may have been caused by nanoclay actions during the spinning and fiber-formation process. Sharper and more distinct peaks also indicated an increase in the crystalline size. Table III gives details about the Bragg angle associated with the individual peaks, interplanar *d*-spacing, and crystal size. The sizes of the crystals were significantly higher in all of the nanoclay-containing samples than in the control PP. These results agreed well with the DSC results of the melting peak shift.

These changes in the crystalline structures (α-crystalline formation and larger crystalline size) could be explained by the effect of nanoclay addition on the crystallization behavior. As explained previously, the nanoclay particles acted as nucleating agents and increased the crystallization rate, which may have caused changes in the crystalline form and crystal size.[20]

TABLE III
Crystallite Sizes of PP and Nanoclay–PP Composites Fibers

Clay type	2θ	*d* (Å)	Crystal size (Å)
PP	15.1	5.86	23
	22.2	4.01	—
PP and 1% nanoclay	15.0	5.89	88
	17.8	4.98	83
	19.5	4.55	96
	22.1	4.01	66
	26.4	3.37	228
PP and 2% nanoclay	14.9	5.94	119
	17.7	5.00	118
	19.4	4.58	109
	21.9	4.05	91
	26.3	3.38	179
PP and 3% nanoclay	14.9	5.94	137
	17.7	5.00	137
	19.4	4.58	115
	26.3	3.38	204

TABLE IV
Birefringence of Nanoclay–PP Composite Fibers

Nanoclay loading	Birefringence
PP control	0.0203
0.5%	0.0196
1.0%	0.0191
1.5%	0.0187
2.0%	0.0184
2.5%	0.0182
3.0%	0.0179

Birefringence

The birefringence of PP and the PP–nanoclay fibers given in Table IV shows that the birefringence of the nanoclay–PP composite fibers was lower than that of the PP fibers. This indicated that the addition of clay particles resulted in a reduction in the molecular orientation of PP molecules. This reduction in the molecular orientation of the fibers highly impacted the mechanical properties of the fibers. However, we still did not fully understand the reason behind these changes. The molecular orientation of a fiber developed during the melt-spinning process is strongly affected by the spinning conditions and also by the polymer-chain properties, including the crystallization behavior.[31] The presence of nanoclay alters the chain rigidity and polymer rheology, so this may hinder the alignment of molecules by spin

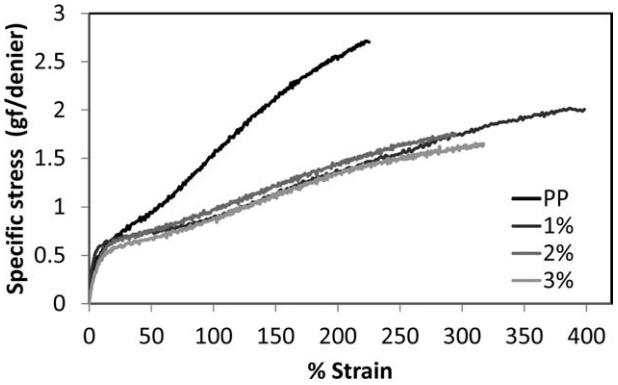

Figure 7 Stress–strain curves of nanoclay–PP composite fibers under tensile deformation.

tension at give spinning speed.[32,33] In addition, changes in the crystallization behavior caused by nanoclay addition could influence the molecular orientation development because crystallization and orientation development occur simultaneously during spinning and they are highly interrelated.[31,34]

Fiber tensile properties

Figure 7 compares the specific stress–strain curves for the PP and nanoclay–PP fiber samples. It was apparent that the addition of nanoclay altered the shape of the stress–strain curve and, thus, the tensile behaviors: it reduced the tenacity and increased the strain at break. In general, the tensile behavior of polymeric fibers is the result of the inherent polymeric chain properties (chain rigidity, secondary bond strength between polymeric chains, and molecular weight of the polymers used) and the microstructures of the fibers formed by polymer-chain alignment. Because the microstructures of fibers were highly dependent on the melt-spinning conditions, the tensile properties in the nanoclay–PP composite fibers were the combined results of the alteration of the polymer-chain properties and microstructural changes. In this case, nanoclay addition in PP were caused by changes in the material properties, which included an alteration in the mobility or rigidity of the polymer chain through intercalation or exfoliation, and the introduction of defect formations when some of the nanoclay formed microcomposite structures. However, as we demonstrated in a previous section, changes in the microstructure were observed with the addition of nanoclay, and this resulted in changes in the crystallization behavior. The shape of the stress–strain curves implicated that the reduction of molecular orientation occurred with the incorporation of

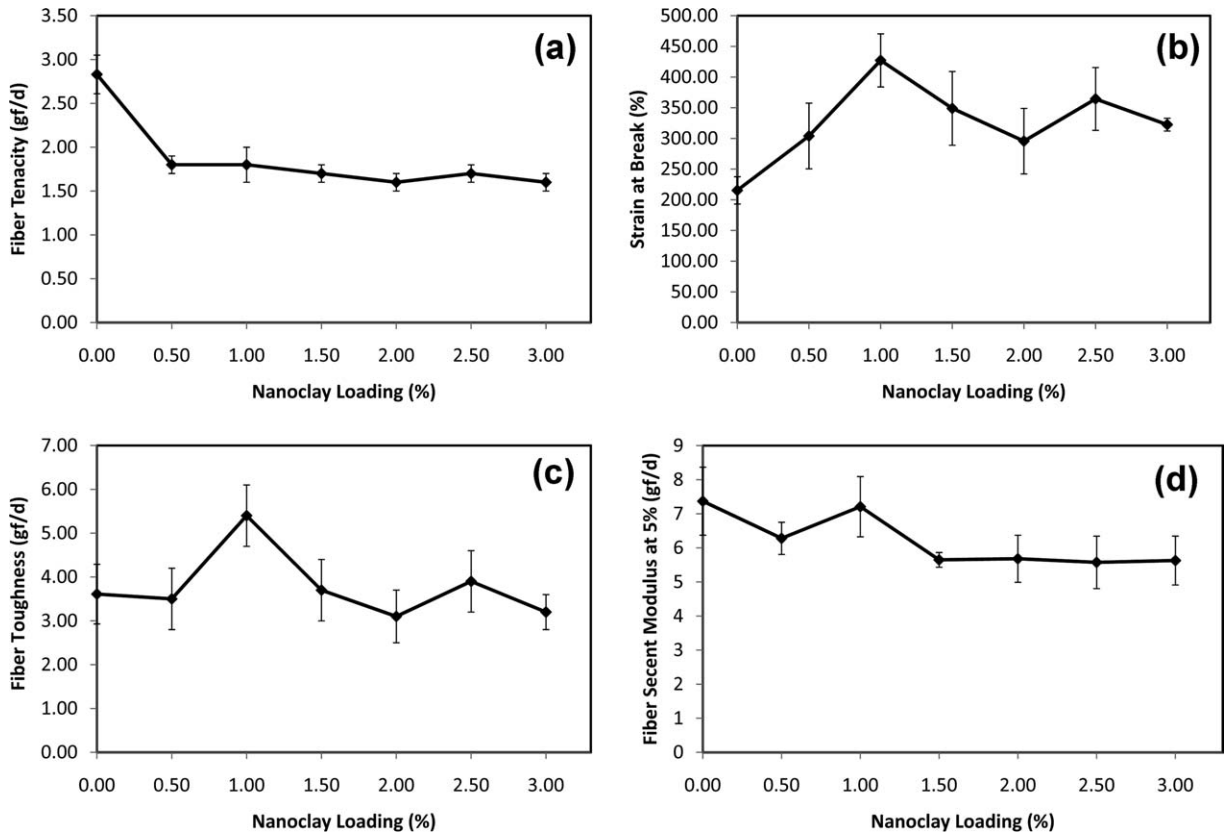

Figure 8 Single-fiber tensile properties of nanoclay–PP fibers: (a) tenacity, (b) strain at break, (c) toughness, and (d) 5% secant modulus.

nanoclay, although all of these fibers were produced with exactly the same spinning conditions. This agreed well with what we observed in the birefringence measurement (Table IV). Regardless of its clay concentration, the fibers with added nanoclay exhibited plateaus after the yield points, where the fibers were elongated greatly without added stress. This is a hallmark behavior of a fiber with an unoriented chain, which realigns parallel to the fiber axis when stressed. This induces an increase in the fiber length without added stress. At a higher clay loading, no further changes in the stress–strain curve were observed, but this caused premature tensile failure compared to the sample with a low clay loading. This may be due to structural defects in the fibers when a high concentration of nanoclay was added. The effect of clay loading on the tensile properties are further summarized in Figure 8, where the tenacity, strain at break, secant modulus at 5%, and toughness were calculated from the stress–strain curves of single fibers. At all clay loading levels, the tenacity was found to be lower than that of PP. There was a greater decrease in the tenacity with increasing clay loading above 1%. As pointed out previously, the reduction of tenacity could be explained by a reduction in the orientation and possible defect formation with the addition of nanoclay. The fiber modulus also exhibited decreasing trends with clay addition. In contrast, the strain at break was dramatically enhanced when nanoclay was added, and it reached its peak at a 1% nanoclay loading level and decreased thereafter. The reduction of orientation could have also been one reason for the higher strain at break in the nanoclay–PP composite fibers. However, the increase in the strain at break was more drastic than changes in the birefringence and fiber tenacity. It reached its peak at the 1% nanoclay loading, where the strain at break almost doubled compared to the PP control. The fiber toughness also increased and reached about 1.5 times that of the PP control at the 1% nanoclay loading. Because the molecular orientation had little impact on the fiber toughness, nanoclay addition in PP caused fundamental changes beyond the alteration of the molecular alignment and led to fibers with more ability to absorb energy before failure. This effect was diminished when the clay loading increased, and the defect formation deteriorated and initiated premature tensile failure. The crystalline structures observed by WAXD (Fig. 6) at the 1% clay loading were significantly different that of the PP control. However, any additional amount of clay changed the X-ray diffraction pattern (Table III) only slightly, and a slight reduction in the crystallinity was also observed.

CONCLUSIONS

Nanocomposites fibers of PP and montmorillonite-based organoclay were produced by a melt-spinning process, and their structures and mechanical properties were studied. Nanoclay addition altered the crystallization kinetics of PP and resulted in changes in the microstructure of the nanoclay–PP composite fibers. Higher n and k values for the nanoclay–PP composite fibers suggested that the nanoclay particles acted as heterogeneous nucleating agents in the polymer matrix and increased the crystallization rate of the host polymer. Nanoclay addition also led to increases in the crystal size, as observed by WAXD and DSC. However, a reduction in the fiber orientation was also observed in the nanoclay–PP nanocomposite fibers and resulted in significant changes in the tensile deformation behavior of fibers. Decreases in the fiber modulus, tenacity, and toughness with increasing strain at break were observed. These changes suggested that nanoclay particles were involved in a fiber-formation process and interacted with polymer chain; then, the composite structures created were highly affected by the material and processing parameters, both on the microscale and nanoscale.

The authors thank Techmer (Clinton, TN) for its assistance and support of this project.

References

1. Brule, B.; Flat, J. J. Macromol Symp 2006, 233, 210.
2. Chen, L.; Wong, S. C.; Pisharath, S. J Appl Polym Sci 2003, 88, 3298.
3. Dasari, A.; Yu, Z. Z.; Mai, Y. W.; Hu, G. H.; Varlet, J. L. Compos Sci Technol 2005, 65, 2314.
4. Drodoz, A. D.; Christiansen, J. D. Eur Polym J 2007, 43, 10.
5. Valera-Zaragoza, A.; Ramirez-Vargas, E.; Medellin-Rodrigues, F. J.; Huerta-Martinez, B. M. Polym Degrad Stab 2006, 91, 1319.
6. Lee, K. Y.; Goettler, L. A. Polym Eng Sci 2004, 44, 1103.
7. Wool, R. P.; Sun, X. S. Bio-Based Polymers and Composites; Elsevier: Boston, 2005.
8. Frounchi, M.; Dadbin, S.; Salehpour, Z.; Noefresti, M. J Membr Sci 2006, 282, 142.
9. Lei, S. G.; Hoa, S. V.; Ton-That, M. T. Compos Sci Technol 2006, 66, 1274.
10. Ton-That, M. T.; Perrin-Sarazin, F.; Cole, K. C.; Bureau, M. N.; Denault, J. Polym Eng Sci 2004, 44, 1212.
11. Ding, C.; Jia, D.; He, H.; Guo, B.; Hong, H. Polym Test 2005, 24, 94.
12. Marchant, D.; Jayaraman, K. Ind Eng Chem Rep 2002, 41, 6402.
13. Kato, M.; Usuki, A.; Okada, A. J Appl Polym Sci 1997, 66, 1781.
14. Kawasumi, M.; Hasegawa, N.; Kato, M.; Usuki, A.; Okada, A. Macromolecules 1997, 30, 6333.
15. Lertwimolnun, W.; Vergnes, B. Polymer 2005, 46, 3462.
16. Wenyi, W.; Xiaofei, Z.; Guoquan, W.; Jianfeng, C. J Appl Polym Sci 2006, 100, 2875.

17. Avella, M.; Cosco, S.; Volpe, G. D.; Errico, M. E. Adv Polym Technol 2005, 24, 132.
18. Joshi, M.; Viswanathan, V. J Appl Polym Sci 2006, 102, 2164.
19. Ma, J.; Zhang, S.; Qi, Z.; Li, G.; Hu, Y. J Appl Polym Sci 2002, 83, 1978.
20. Zhang, X.; Yang, M.; Zhao, Y.; Zhang, S.; Dong, X.; Liu, X.; Wang, D.; Xu, D. J Appl Polym Sci 2004, 92, 552.
21. Seo, Y.; Kim, J.; Kim, K. U.; Kim, Y. C. Polymer 2000, 41, 2639.
22. Varga, J. In Polypropylene: Structure, Blends and Composites; Karger-Kocsis, J., Ed.; Chapman & Hall: London, 1995; Vol. 1, Chapter 3.
23. Svoboda, P.; Zeng, C.; Wang, H.; Lee, L. J.; Tomasko, D. J. J Appl Polym Sci 2002, 85, 1562.
24. Qian, G.; Lan, T.; Fay, A. M.; Tomlin, A. S. U.S. Pat. 6,462,122 (2002).
25. Qian, G.; Cho, J. W.; Lan, T. U.S. Pat. 6,632,868 (2003).
26. Karger-Kocsis, J. Polypropylene Structures, Blends and Composites—Structure and Morphology; Chapman & Hall: London, 1995.
27. Cullity, B. D.; Stock, S. R. Elements of X-Ray Diffraction; Prentice-Hall: Upper Saddle River, NJ, 2001.
28. Frounchi, M.; Dourbash, A. Macromol Mater Eng 2009, 294, 68.
29. Avrami, J. J Chem Phys 1939, 7, 1103.
30. Avrami, J. J Chem Phys 1940, 8, 212.
31. White, J. L.; Cakmak, M. Adv Polym Technol 1986, 6, 295.
32. Peltola, P.; Vallpakka, E.; Vuorinen, J.; Syrjaia, S.; Hanhl, K. Polym Eng Sci 2006, 46, 995.
33. Solomon, M. J.; Almusallam, A. S.; Seefeldt, K. F.; Somwangthanaroj, A.; Varadan, P. Macromolecules 2001, 34, 1864.
34. Katayama, K.; Nakamura, K.; Amano, T. Kolloid-Z Z Polym 1968, 226, 125.